Polyhedron 199 (2021) 115048

Contents lists available at ScienceDirect

Polyhedron

journal homepage: www.elsevier.com/locate/poly

Oxidative cyclization and synthesis of benzoxazole derivatives and hydrolytic phosphatase activity studies on dinuclear diphenoxo-bridged zinc(II)complexes

Kapil Kumar, Virendra Kumar Chaudhary, U.P. Singh, Kaushik Ghosh

Department of Chemistry, Indian Institute of Technology Roorkee, Roorkee 247667, Uttarakhand, India

ARTICLE INFO

Article history:
Received 21 November 2020
Accepted 12 January 2021
Available online 31 January 2021

Keywords:
Dinuclear diphenoxo bridged Zn(II) complexes
Crystal structure
Phenoxyl radical complex
Phosphatase activity
Oxidative cyclization and benzoxazole synthesis

ABSTRACT

Diphenoxo bridged dinuclear zinc complexes, $[Zn_2(Phimp)_2(Cl)_2]$ (**1**) (PhimpH = (E)-2-((2-phenyl-2-(pyridin-2-yl)hydrazono)methyl)phenol), $[Zn_2(Me\text{-}Phimp)_2(Cl)_2]$ (**2**) (Me-PhimpH = (E)-4-methyl-2-((2-phenyl-2-(pyridin-2-yl)hydrazono)methyl)phenol), $[Zn_2(OMe\text{-}Phimp)_2(Cl)_2]$ (**3**) (OMe-PhimpH = (E)-4-methoxy-2-((2-phenyl-2-(pyridin-2-yl)hydrazono)methyl)phenol), were synthesized and spectroscopically characterized. The molecular structure of **2** was determined using X-ray crystallography. DFT and TD-DFT calculations were performed to optimize the molecular geometry, interpret the spectroscopic results and investigate the contribution of the ligands to the redox properties of the complexes. Phenoxyl radical complexes were generated in solution via chemical oxidation using ceric ammonium nitrate (CAN) and the redox properties were examined through cyclic voltammetric measurements. The hydrolysis of *para*-nitrophenylphosphate (PNPP) by all the dinuclear zinc complexes was investigated to mimic phosphatase activity. Catalytic oxidative cyclization by these complexes and synthesis of benzoxazole derivatives was investigated.

1. Introduction

The zinc(II) ion, having filled d-orbitals (d^{10} electronic configuration), exhibits some dissimilar properties compared to other first row transition metals, such as redox inactivity and magnetic properties [1]. Interestingly, strong Lewis acidity and a capability for ligand exchange are two important properties for this metal ion. The parallel chemistry of zinc always helps to understand the chemistry of copper as both possess a stable 2 + oxidation state [2]. The chemistry of zinc containing dinuclear diphenoxo bridged complexes has received considerable attention and these complexes were synthesized and characterized for different objectives [2–21]. First, dinuclear diphenoxo bridged complexes were utilized for functional mimicking of phosphatase [3–8] nuclease [2,9] catecholase [9,10] and phenoxazinone synthase [10] enzymes. Second, a few research groups were interested in designing and synthesizing these complexes for polymerization reactions [11–15] because they are found to be efficient catalysts for different polymerization reactions. Third, a few groups were interested in synthesizing dinuclear zinc complexes for some specific applications. In this regard we would like to mention that Williams and co-workers investigated aggregation induced fluorescence properties [16] whereas photophysical properties were also studied in a few reports [17–19]. Akitshu and coworkers [20] utilized zinc complexes as fluorescent probes for the CD19 antibody protein. Mugesh and coworkers [21] are interested in studies on interactions with β-lactamase. As a part of our ongoing research on structural and functional mimicking of the galactose oxidase enzyme, we have been working with dinuclear zinc complexes to understand the non-innocent properties of the phenolate ligand and generation of phenoxyl radical complexes [2,10]. Investigation of the mechanism [22] indicated that a copper coordinated phenoxyl radical could abstract a H atom [23–25]. This prompted us to study the HAT (hydrogen atom transfer) reaction of dinuclear diphenoxo bridged complexes and to try and utilize this phenomenon for some organic transformations.

Herein, we report the synthesis and characterization of three dinuclear diphenoxo bridged zinc complexes, $[Zn_2(Phimp)_2(Cl)_2]$ (**1**), $[Zn_2(Me\text{-}Phimp)_2(Cl)_2]$ (**2**) and $[Zn_2(OMe\text{-}Phimp)_2(Cl)_2]$ (**3**) derived from the ligands PhimpH, Me-PhimpH and OMe-PhimpH respectively (shown in Scheme 2). These complexes were characterised by different spectroscopic methods and the molecular structure of $[Zn_2(Me\text{-}Phimp)_2(Cl)_2]$ (**2**) was determined by X-ray crystallography. To investigate the hydrolytic properties of these complexes and functional mimicking of phosphatase enzyme, we have examined the phosphatase activity. On the other hand, the presence of a non-innocent phenolate function prompted us to

E-mail addresses: kaushik.ghosh@cy.iitr.ac.in, ghoshfcy@iitr.ac.in (K. Ghosh)

https://doi.org/10.1016/j.poly.2021.115048
0277-5387/

study the synthesis of benzoxazole derivatives by dehydrogenative cyclization. Conversion of dihydroanthracene to anthracene will be scrutinized in light of the HAT reaction.

2. Results and discussion

2.1. Synthesis and characterization of the ligands

The ligands PhimpH, Me-PhimpH and OMe-PhimpH (Scheme 1) have been synthesized by the following literature procedure [10] and satisfactorily characterized by IR, UV–Vis and ^{1}H NMR spectroscopic studies.

2.2. Synthesis and characterization of the zinc complexes

The Schiff-base ligands were synthesized by refluxing a 1:1 mixture of the corresponding substituted aldehyde and 2-(1-phenylhydrazinyl)pyridine in methanol [10]. Generally, yellow coloured ligands were produced in good to excellent yields. All three complexes were synthesized by the reaction between the Schiff-base ligands and anhydrous zinc chloride in a 1:1 M ratio, which yielded yellowish coloured compounds (Scheme 2). We found that the complexes are highly soluble in organic solvents, such as acetonitrile (ACN), dichloromethane (DCM), chloroform and N,N-dimethylformamide (DMF). The zinc complexes were characterized by different analytical and spectroscopic techniques. The IR spectra of the three complexes exhibited a strong band in the range 1628–1640 cm^{-1} (Figs. S1, S2 and S3). These bands were assigned to $\nu_{C=N}$, which suggested the coordination of these ligands to the metal ions through the imine nitrogen atoms [10].

The UV–visible spectroscopic studies were performed to evaluate the electronic properties of all the synthesized zinc complexes. The electronic spectra of the complexes (**1**, **2** and **3**) in acetonitrile solvent are shown in the supporting information (Fig. S4). The absorption bands observed in the range 300–391 nm for the complexes are assigned to the n-π^* and π-π^* intra-ligand transitions [10]. All the zinc complexes showed a band near 300–400 nm, which clearly indicated ligand to the metal charge transfer transitions [10].

The ^{1}H and ^{13}C NMR spectra of Me-PhimpH and complex **2** are shown in Figs. S22, S23, S24 and S25 respectively. For complex **2**, the observed peaks between δ 6.5 and 7.6 ppm were found to be due to the aromatic hydrogen atoms. Multiplet signals of methylene hydrogen atoms were found in the range $\delta \approx 1.2$–2.5 ppm.

2.3. Description of the molecular structure of complex *2*

Yellow crystals of complex **2** were grown from a 1:1 solution of acetonitrile and dichloromethane, and the crystals were obtained

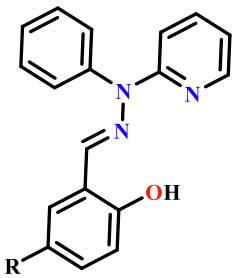

Ligand = R-PhimpH
R = H, Me, OMe

Scheme 1. Schematic drawing of the ligands.

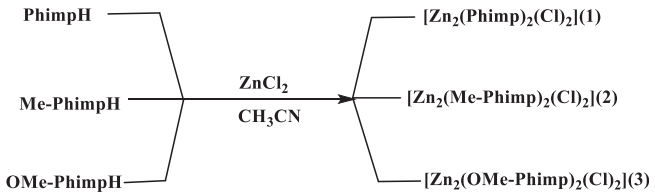

Scheme 2. Synthetic drawing for the synthesis of complexes **1**–**3**.

using the slow evaporation method. To confirm the structure of complex **2** and the mode of coordination of the ligand (Me-Phimp)$^{1-}$, single-crystal X-ray structure determination for complex **2** was carried out. The molecular structure of the diphenoxo-bridged dinuclear zinc complex **2** is shown in Fig. 1. The parameters of the metal complex are given in Table S1, whilst selected bond angles and bond distances are described in Table S2.

The crystal structure (Fig. 1, Tables S1 and S2) reveals that complex **2** adopts a dinuclear structure, consisting of two pentacoordinated zinc(II) ions bridged by two phenolato functional groups. To describe the geometry around the pentacoordinated zinc(II) centre, we have calculated the structural index parameter τ for complex **2** [26]. The τ values were found to be 0.24 and 0.01 for the Zn1 and Zn2 centers respectively, and these results clearly show a distorted square pyramidal geometry around the pentacoordinated zinc centres in complex **2**. For the metal centre Zn1, one imine nitrogen atom (N6), two bridged phenolato oxygen atoms (O1 and O2) and and one pyridine nitrogen atom (N4) constitute the equatorial plane, whereas the axial position is occupied by a chloride ion (Cl1). Similarly, for the other metal centre, Zn2, one imine nitrogen atom (N3), one pyridine nitrogen atom (N1) and two bridged phenolate oxygen atoms (O1 and O2) constitute the equatorial plane, and the other chloride ion (Cl2) occupies the axial position.

Herein, we observed that in complex **2**, the two chloride ions Cl1 and Cl2 are on the same side of the Zn-Zn axis, Consequently the ligands (Me-Phimp)$^-$ occupy the other side of the metal ions, giving rise to an overall unique *cis* configuration in complex **2**.

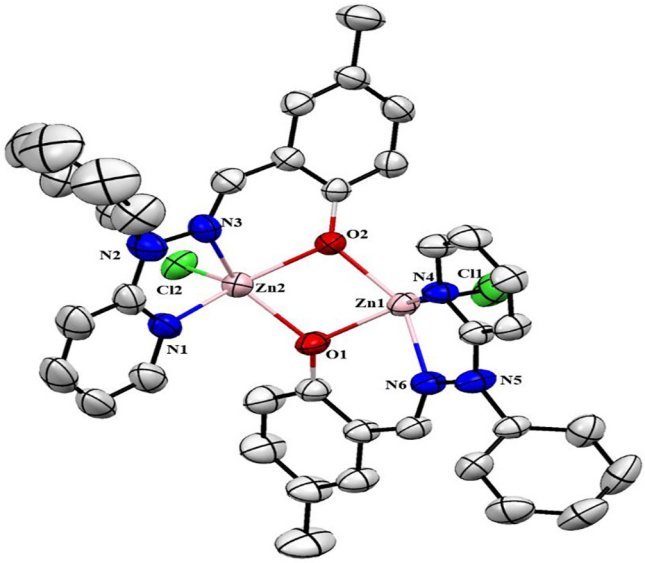

Fig. 1. ORTEP diagram (40% probability level) of the complex [Zn_2(Me-Phimp)$_2$(-Cl)$_2$] (2). Hydrogen atoms are omitted for clarity. Selected bond lengths (Å): Zn1-Zn2 3.1199(4), Zn1-O1 2.0217(16), Zn1-O2 2.0390(15), Zn1-N6 2.180(2), Zn1-Cl1 2.2091(8), Zn2-O1 2.0438(15), Zn2-O2 2.0208(15), Zn2-N1 2.090(2), Zn1-N4 2.0892 (18), Zn2-Cl2 2.2307(7), Zn2-N3 2.201(2).

The axial distances Zn1-Cl1 and Zn2-Cl2 are 2.209 and 2.231 Å respectively. The cis arrangement of the chloride ions with respect to the Zn-Zn axis is different to the structure reported by Reedijk et al. [26] which is consistent with the previously reported data [2]. All the Zn-N ($N_{pyridine}$ as well as N_{imine}) distances are consistent with the data reported by Reedijk and coworkers [26]. We have reported that Zn-Zn distances in these types of complexes are observed in the range 2.94–3.24 Å [10]. The Zn-Zn distance obtained for complex **2** (3.119 Å) was found to be on the higher side of the range. The Zn-Zn bond length in complex **2** is most similar to the reported data of Williams and coworkers [12]. However, the distance is higher than the values reported by Nordlander and coworkers [7] and smaller than those reported by Mukherjee and coworkers [4] and Sharma and coworkers [5]. For complex **2**, the Zn-O (phenolato) bond lengths are found to be in the range 2.0208 to 2.0438 Å (Table S2).

These observed distances are very similar to our previous results [2,10], data published by Reedijk and coworkers [26] and Das and coworkers [27]. The Zn-O-Zn bond angles of the phenoxo bridged moiety are observed in the range 100.24–100.44°, whilst the O-Zn-O bond angles are observed in the range 78.72–78.82°. Non-covalent interactions, hydrogen bonding networks and π-stacking interactions play important roles in biology, supramolecular chemistry and crystal engineering [28–30]. In complex **2**, intermolecular hydrogen bonding interactions are observed between the aryl hydrogen atoms of the phenyl ring and the chloride ions (Fig. S5).

2.4. Computational studies

Density functional theory (DFT) calculations were performed to find a correlation between the experimental and obtained results from theoretical assumptions of all the dinuclear zinc complexes by utilizing the B3LYP functional approach and the LANL2DZ basis set. The Chemcraft and Gauss View 5.0 programs were used for the formation of HOMO-LUMO orbitals (Fig. S6). The main purpose of performing computational studies was to confirm the site of the electronic distribution or electron loss on the ligand part of the complex. Electron density distribution analysis was carried out with the Gauss Sum software [31–32]. The frontier molecular orbital compositions and energy levels of complex **2** in the singlet ground state are shown in Table S4, whilst the data for complexes **1** and **3** were reported in our previous results [10]. It is important to mention that in all the zinc complexes, the electron density in the HOMO orbital mainly originates on the ligand part and the contribution from the metal centres in the HOMOs of complexes **1**–**3** was found to be negligible, which revealed the non-innocent behaviour of the ligands [10]. We also observed that the contribution of the ligand without the phenolato ring was found to be about 34% in all the three complexes. In the HOMO, the contribution of the phenyl ring containing the phenolato function is around 56% and the remaining 44% electron density is dispersed over the imine and pyridine moieties for complex **2**. In the LUMO state, the ligand afforded a contribution of around 54% for the phenolato ring of complex **2** and remaining 46% electron density is localized over the imine and pyridine moieties. However, we have observed a 23% contribution for the phenolato ring in the LUMO state of complexes **1** and **3** [10].

The results of these calculations, revealing that around 56% of the electron density for the HOMO is localized for the phenyl ring containing the phenolato function in **2**, indicate that the phenol function could afford radical generation. The LUMO states of all the dinuclear zinc complexes originate from the π* orbital character of the whole ligand, however orbitals L + 4 and L + 5 originate from the ligand part, but with 0% character of the phenolato moiety of the ligand. There is a small difference between the HOMO-LUMO gap, corroborating the value of 3.40 eV found for complex **2**. Similarly, complexes **1** and **3** behave like complex **2** due to small energy differences [10] between the HOMO and LUMO, with small shifts in the absorption bands, and this result also correlates well with the experimental results.

Time-dependent density functional theory (TD-DFT) was used to evaluate the origin of the electronic properties of all the dinuclear zinc complexes and to explain the UV–visible spectral data. The data obtained for complex **2** from the TD-DFT calculations are shown in Table S5. However, the TD-DFT data of complexes **1** and **3** are given in our previous results [10]. Four main electronic transitions were observed for complex **2**. These main transitions are (1) $S_0 \rightarrow S_4$ (H-1 → L + 1), 375 nm, f = 0.1619, (2) $S_0 \rightarrow S_7$ (H → L + 3), 342 nm, f = 0.0843 (3) $S_0 \rightarrow S_9$ (H-2 → L + 1), 312 nm, f = 0.3172 and (4) $S_0 \rightarrow S_{40}$ (H-3 → L + 1), 265 nm, f = 0.1205. These transitions can be assigned to ILCT ($p\pi \rightarrow p\pi^*$) transitions in the spectrum [10]. The probable electronic transitions of complex **2** are shown in Fig. S7.

2.5. Electrochemistry

The redox behaviour of the zinc complexes **1**–**3** was investigated by a cyclic voltammetric study, the data is deposited in Table S3 and the voltammograms are displayed in Fig. S8. Complexes **2** and **1** showed quasi-reversible redox waves centred at $E_{1\backslash 2}$ = 1.00 and 0.841 V vs Ag/AgCl respectively. On the other hand, complex **3** displayed $E_{1\backslash 2}$ at 0.663 and 1.13 V. These are probably due to the successive oxidation of the phenolate function to the phenoxyl radical [10].

2.6. Generation of the phenoxyl radical

Phenoxyl radical species were generated by the addition of CAN to an acetonitrile solution of the complexes. Generation of phenoxyl radicals from complexes **1**–**3** after the addition of CAN was analyzed by a UV–Vis spectrophotometer. A representative spectrum for complex **2** is shown in Fig. 2 (A). The spectra for complexes **1** and **3** are given in our previously reported results [2,10]. A UV–visible spectral studies were utilized for the detection of phenoxyl radical complexes, by performing oxidation of complexes **1**, **2** and **3** after addition of CAN. After the addition of an acetonitrile solution of CAN to an acetonitrile solution of complex **2**, the band at 334 nm disappeared. A new band at 300 nm and broad band of low intensity at around 800 nm were observed. These observations clearly indicate the formation of a phenoxyl radical at 0 ºC [2,10].

Further, generation of phenoxyl radicals by the addition of CAN to an acetonitrile solution of complex **2** was also confirmed by EPR spectroscopic studies. After the addition of CAN to an acetonitrile solution of complex **2**, a sharp band near the value g = 1.997 was obtained, that clearly indicates the generation of a phenoxyl radical [2,10] in the solution (Fig. 2(B)).

3. Reactivity studies

3.1. Phosphatase activity

Earlier we have described that the dinuclear zinc complexes **1**–**3** have two chloride ions which are *cis* to each other, and both the zinc centres are separated from each other by distances in the range 3.118–3.178 Å. This prompted us to study the phosphatase activity with all the zinc complexes utilizing the disodium salt of 4-nitrophenyl phosphate hexahydrate (4-NPP) as a substrate (Scheme 3). The hydrolytic tendency of complexes **1**–**3** was measured spectrophotometrically by monitoring the time evolution

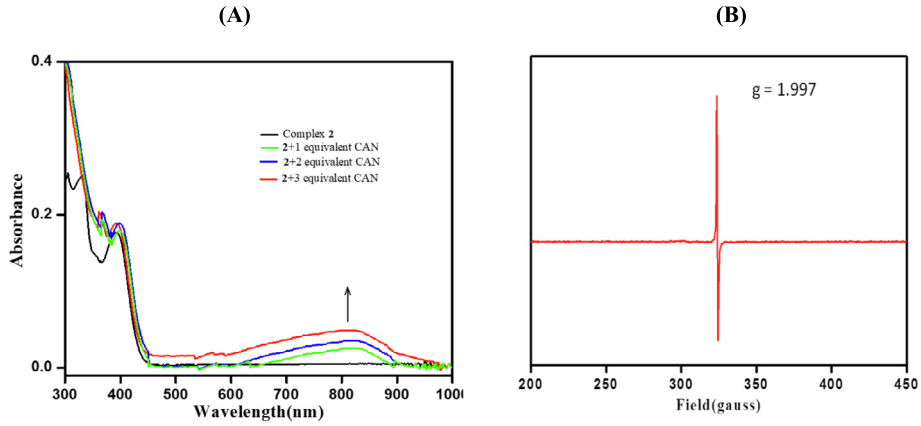

Fig. 2. (A) Generation of the phenoxyl radical from **2** (10×10^{-5}M) after addition of CAN (-1 equivalent, -2 equivalents and -3 equivalents) in acetonitrile solvent at 0 °C. (B) EPR spectrum of complex **2** recorded at 298 K after addition of CAN in acetonitrile.

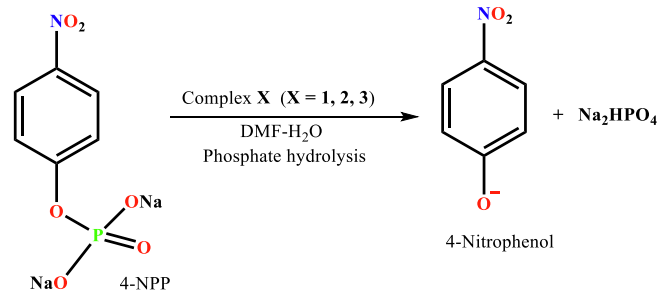

Scheme 3. A schematic depiction of the phosphate hydrolysis reaction of 4-NPP-catalysed by the dinuclear zinc(II) complexes.

of 4-nitrophenolate band at 423 nm through a wavelength scan in the DMF/H_2O solvent system [33a]. The changes in the spectral features of **1**–**3** upon the addition of PNPP are shown in Fig. 3 as representative scans.

The kinetic investigation of the zinc complexes **1**–**3** were carried out by the initial slope method, monitoring the growth of the p-nitrophenolate band at 423 nm as a function of time over 2 h. The initial rate constant for a particular complex and substrate mixture was determined from the log [Aα/(Aα – At)] *vs* time plot (Fig. S9) for all the zinc complexes.

In all cases, a first-order kinetic dependence was observed at low concentrations of 3,5-DTBC, whereas higher concentrations resulted in saturation kinetics.

The observed rates versus concentration of substrate data were analyzed and then based on the Michaelis Menten approach of enzymatic kinetics (Fig. S10), the kinetic parameters V_{max}, K_M, K_{cat} for of the dinuclear zinc complexes were investigated from a Lineweaver-Burk (double reciprocal) plot of 1/V versus 1/[S] (Fig. S11). All the kinetic parameters are given in Table 1.

The catalytic activity order of the complexes, **2** > **3** > **1**, demonstrates a direct correspondence to the Zn. . .Zn separation (3.170 Å for **1**, 3.119 Å for **2** and 3.155 Å for **3**), showing the shorter Zn. . .Zn separation is better more qualified to accommodate the phosphate group [33a]. Also, the catalytic activity of complex **2** is better than some reports available in the literature [5].

*3.2. Catalytic activity of the complexes **1**, **2** and **3** for the synthesis of benzoxazole derivatives*

The H• abstraction tendency of the phenoxyl radical was utilized in our previous results for benzyl alcohol oxidation, and catechol and o-aminophenol oxidase activity [10]. Herein, we have further employed the H· abstraction tendency of the phenoxyl radical for the C—H bond. Activation of the imine substrate resulted in benzoxazole derivatives *via* the formation of a C—O bond. Previously, we reported the synthesis of benzoxazole by nitric oxide *via* a radical-mediated mechanism [34a] which clearly expresses the role of radical species (phenoxyl) in the HAT (hydrogen atom transfer) mechanism [23–25]. In search of effective conditions for the non-toxic, environmentally benign synthesis of benzoxazole derivatives, being homogeneously catalysed [34b,c] by complexes **1**, **2** and **3** (Scheme 4), we selected the reaction of Schiff bases derived from 2-amino phenol and substituted benzaldehydes (1 mmol) as a model reaction to optimize the reaction conditions (Table 2).

All the substrates, decorated with electron-withdrawing or electron-donating groups on the aromatic ring, tolerate varieties of functional groups. A full report on the effect of solvents, catalysts, reaction time and catalyst loading on the synthesis of benzoxazole is also provided in Table 2. A blank reaction without catalyst was also performed to ascertain the role of the complexes in the hydrogen atom abstraction; no product was detected.

We started the reaction by taking 0.2 mol% of the catalyst (complex **1**, **2** or **3**) at 60 °C in acetonitrile solvent. These reactions, catalysed by complexes **1**, **2** and **3**, yielded 48, 54 and 55% of benzoxazole after 12 h. It was observed that complex **1** exhibited comparatively lower catalytic activity than **2** and **3**. A change of the solvent from acetonitrile to DMF-H_2O (1: 9) at 60 °C, gave rise to only 7, 11 and 13% yields of product formation for catalysts **1**, **2** and **3** respectively. To shorten the time and enhance the product yield, the reaction was performed in the presence of additives. The addition of TEMPO enhanced the catalytic activity, which was clearly observed from the product yields [23]. TEMPO can act as an oxidizing agent as well as a radical scavenger. Hence, the enhancement of the product yield in the presence of TEMPO could be because TEMPO might generate more phenoxyl radical species in solution by a one-electron oxidation of the phenolate group of ligand, which in turn abstract H• from the substrate molecules. Notably, only 18% yield of benzoxazole was observed in the presence of 3 mol% of TEMPO in the absence of catalysts. However, 3 mol% of TEMPO in the presence of 0.2 mol% of catalysts **2** and **3** afforded 79–94% product yield at 60 °C after 12 h. Similarly, complex **1** produced 68% yield of benzoxazole. Different solvents were also tested, but no appreciable changes in the product yield were observed. It was observed that the reaction at room temperature was very slow and it took a longer time to afford benzoxazole with

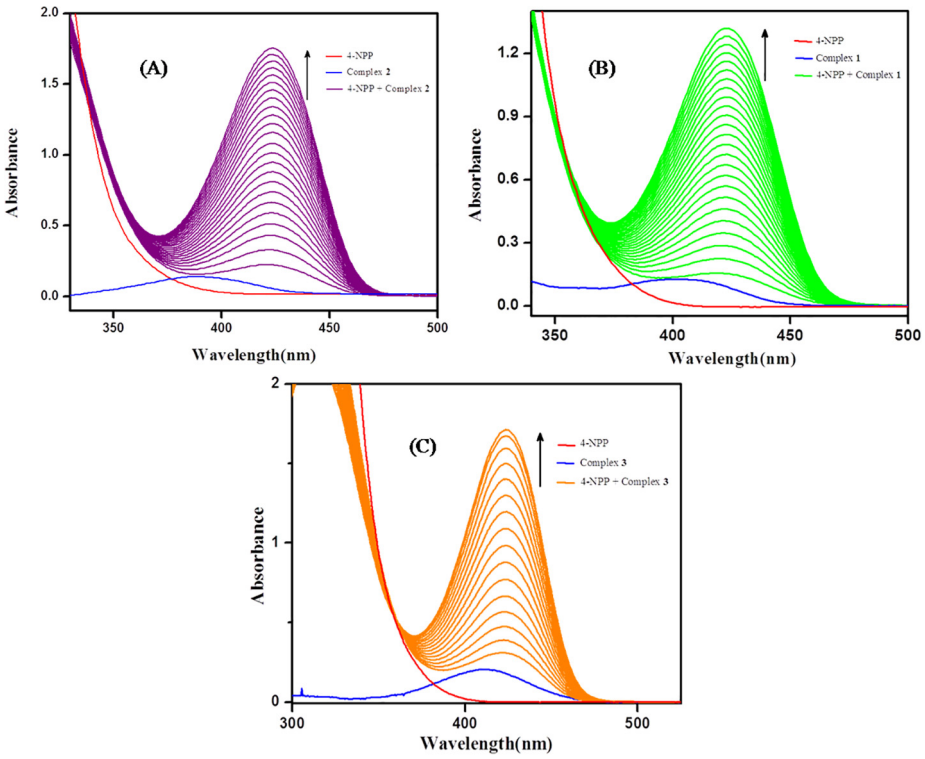

Fig. 3. (A) Wavelength scan for the hydrolysis of 4-NPP in the absence and presence of complex **2** (substrate:catalyst = 20:1) in solution (97.5% DMF and 2.5% H_2O) recorded at 25 °C after intervals of 5 min. [4-NPP] = 1×10^{-3} M; [complex **2**] = 0.05×10^{-3} M, (B) for complex **1**, (C) for complex **3**. The arrow shows the change in absorbance with the reaction time.

Table 1
Kinetic parameters for the hydrolytic cleavage of PNPP catalyzed by **1**–**3** in aqueous DMF at 25 °C.

Complex	V_{max} (M s^{-1})	K_m (M)	k_{cat} (h^{-1})
1	4.9×10^{-4}	7.8×10^{-3}	1.78×10^{4}
2	11.64×10^{-4}	9.59×10^{-3}	4.1×10^{4}
3	7.7×10^{-4}	9.6×10^{-3}	2.77×10^{4}

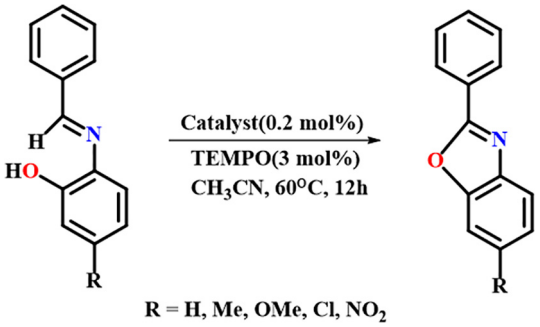

Scheme 4. Synthesis of benzoxazole from 2-(benzyledeneamino)phenol [catalyst = zinc complexes **1**, **2** and **3**].

55% and 43% yields using complexes **2** and **3** respectively after 24 h.

On increasing the catalyst loading at room temperature, the product yield was increased to some extent.

Under the optimized reaction conditions, different types of benzoxazole derivatives were synthesized (Table 3). Herein, we used two different derivatives of *o*-aminophenol, one with a substituent at the *para*-position to phenol and the other one is un-substituted *o*-aminophenol. Substitution of a methyl group at the *para*-position of phenol did not show any difference in the product yield. Electron-withdrawing substituents, such as -Cl and -NO_2 groups on the aryl ring, yielded products in excellent yields as compared to electron-donating groups like-Me and -OMe substituted on the aryl ring.

Table 2
Optimization of the reaction conditions for the synthesis of benzoxazole.

Entry	Catalyst	Additive	Solvent	Yield (%)
1	**1**	__	DMF + H_2O	7
2	**2**	__	DMF + H_2O	11
3	**3**	__	DMF + H_2O	13
4	**1**	__	CH_3CN	48
5	**2**	__	CH_3CN	54
6	**3**	__	CH_3CN	55
7	**1**	TEMPO	CH_3CN	68
8	**2**	TEMPO	CH_3CN	79
9	**3**	TEMPO	CH_3CN	94
10	–	TEMPO	CH_3CN	18

4. Conclusion

Following are the major findings and conclusions of our present study:

1. Dinuclear zinc complexes **1**–**3** have been synthesized by utilizing tridentate ligands and were characterized. The molecular structure of the representative complex **2** was determined by X-ray crystallography.
2. DFT calculations clearly indicate the non-innocent property of the phenolate function and phenoxyl radical complexes were generated in solution. Complex **3** provided the most stable phenoxyl radical complex, whereas **1** gave rise to the least stable one.

Table 3
Substrate scope for benzoxazole synthesis.

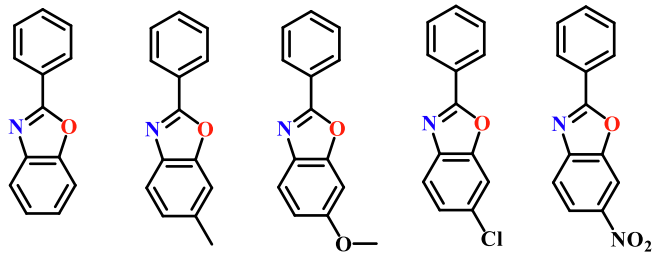

3a 3b 3c 3d 3e

Conditions: imine substrates (1 mmol), catalyst (0.2 mol%), TEMPO (3 mol%), solvent (acetonitrile 5 mL), time = 12 h.

3. Functional mimicking of phosphatase enzyme was investigated by studying the hydrolysis of disodium 4-nitrophenyl phosphate (4-NPP).
4. These complexes were exploited as homogeneous catalysts for the synthesis of benzoxazole derivatives via oxidative cyclization. The hydrogen atom abstraction ability of the phenoxyl radical complexes were utilized to achieve the synthesis of benoxazole derivatives from Schiff bases of benzaldehyde and o-aminophenol. H· abstraction and C—H bond activation of the imine carbon atom resulted in C—O bond formation.

The application of these complexes for other catalytic activities are under progress.

5. Experimental

5.1. Materials

All the chemicals were purchased from commercial sources and used as received. Using standard procedures, the solvents were distilled prior to use. All solvents used for spectroscopic studies were HPLC grade. Analytical grade reagents, sodium hydride (Acros), salicylaldehyde (SRL), 2-hydroxy-5-methoxylbenzaldehyde and 2-hydroxy-5-methylbenzaldehyde were prepared according to the literature [35]. Disodium (4-nitrophenyl)phosphatehexahydrate (4-NPP), (Avra Synthesis) was used as purchased. The analytical grade reagents anhydrous $ZnCl_2$ (Merck limited Mumbai), cerric ammonium nitrate and benzaldehyde (Himedia), and TEMPO (Sigma Aldrich) were used as purchased.

5.2. Methods

Elemental analyses were carried out microanalytically with an Elemenlar Vario EL III. Infrared spectra were recorded on a Thermo Nicolet Nexus FTIR spectrophotometer and were obtained in KBr pellets using 16 scans (in cm^{-1}). Electronic absorption spectra of all the ligands and metal complexes were obtained with an Evolution 600, Thermo Scientific UV–Vis spectrophotometer. ^1H NMR spectra were taken in deuterated solvents on a Bruker AVANCE, 500.13 MHz spectrometer. EPR spectra were taken on a Bruker EMX EPR spectrometer. The cyclic voltammetric study was performed on a CH-600 electro analyzer in dichloromethane solution with 0.1 M tetrabutylammonium perchlorate (TBAP) as the supporting electrolyte. The working electrode, reference electrode and auxiliary electrode were a glassy carbon electrode, Ag/AgCl electrode and Pt wire respectively. The concentration of the compound was $\sim 10^{-3}$ M. The ferrocene/ferrocenium couple appeared at $E_{1/2}/V(\Delta E_p/mV) = +0.46(143)$ *vs.* Ag/AgCl (scan rate 0.1 V/s) in dichloromethane under the same experimental conditions.

5.3. X–ray crystallography

A yellow coloured crystal of zinc complex **2** was used for the determination of the solid-state structure. The X-ray diffraction data of the metal complex was obtained at 273 K on a Bruker Kappa Apex-II CCD diffractometer, with the use of graphite monochromatic Mo-Kα radiation (λ = 0.71073 Å). The structure solution, refinement and data outputs were carried out with the help of the SHELXTL program [36]. To refine the hydrogen and non-hydrogen atoms, isotropic and anisotropic thermal parameters were used respectively. The image was created with the help of the MERCURY 3.7 program. The crystal data and other relevant information are given in the ESI (Table S1).

5.4. Computational details

Theoretical calculations were carried out for all the ligands, namely PhimpH, Me-PhimpH and OMe-PhimpH, as well as their binuclear zinc complexes **1**, **2**, and **3**. DFT and TD-DFT calculations [37–39] were carried out on the optimized geometrical structure (Fig. S22) by utilizing the B3LYP functional approach and the LANL2DZ basis set [40]. The TDDFT technique yielded progressively the exact electronic excitation energies. The HOMO-LUMO were prepared by utilizing the Gauss View 5.0 software [41]. All the DFT calculations were performed with the assistance of the Gaussian 09 W software [42]. Gauss Sum 2.1 was utilized to determine the percentage contributions from groups or atoms in the molecular orbitals.

5.5. EPR spectroscopy

X-band EPR spectra were obtained on a Bruker EMX EPR spectrometer with the following spectrometer settings: microwave frequency, 9.44 GHz; microwave power, 1 mW; modulation frequency, 100 kHz; modulation amplitude, 5G.

6. Synthesis and characterization of the ligands and metal complexes

6.1. Syntheses of the ligands

The ligands PhimpH, Me-PhimpH and OMe-PhimpH were synthesized by the previously reported experimental method [33b]. The substituted salicylaldehydes were synthesized by the formylation of the corresponding phenols using a previously reported procedure [35]. The NMR spectra of the ligand Me-PhimpH are shown in the supporting file (Figs. S23-S24).

6.2. Syntheses of the metal complexes

6.2.1. Synthesis of $[Zn_2(Phimp)_2(Cl)_2]$ (**1**)

To a solution of PhimpH (0.145 g, 0.5 mmol) in acetonitrile (10 mL), sodium hydride (0.012 g, 0.5 mmol) was added consecutively in acetonitrile, and the resulting solution was stirred for 40 min. A solution of anhydrous $ZnCl_2$ (0.085 g, 0.5 mmol) in acetonitrile was then added to the reaction mixture with constant stirring. After 8 h stirring, a yellow-colored complex precipitated out. The solvent was evaporated and the solid was separated by filtration. A yellow-colored compound resulted after redissolving the solid in methanol, then layering this solution with hexane. This compound was washed with diethyl ether and dried under air. Yield: 76%. Anal. Calcd for $C_{36}H_{28}N_6Cl_2O_2Zn_2$: C, 55.55; H, 3.63; N, 10.80. Found: C, 55.38; H, 3.72; N, 10.64. IR (KBr pellets, cm^{-1}): ν(C=N), 1637, 1571, 1483, 1440, 1346, 1306, 1218, 1146, 1056, 958, 879, 811, 772, 697, 564. UV–vis (CH_3CN $\lambda_{max,}$ nm (ε, in M^{-1} cm^{-1})): 335 (50939), 307 (35606), 235 (28290).

6.2.2. Synthesis of $[Zn_2(Me\text{-}Phimp)_2(Cl)_2]$ (**2**)

This compound was prepared by following the same procedure as described above for **1**, except using Me-PhimpH instead of PhimpH. The NMR spectra of complex **2** are shown in the supporting file (Fig. S25-S26). Yield: 72%. Anal. Calcd for $C_{38}H_{32}N_6Cl_2O_2Zn_2$: C, 56.60; H, 4.00; N, 10.42. Found: C, 56.47; H, 4.23; N, 10.32. IR (KBr pellets, cm^{-1}): ν(C=N), 1633, 1562, 1480, 1423, 1331, 1315, 1290, 1021, 851, 752, 700, 554. UV–vis (CH_3CN $\lambda_{max,}$ nm (ε, in M^{-1} cm^{-1})): 373 (29444), 332 (36666), 301 (38888), 246 (48666).

6.2.3. Synthesis of $[Zn_2(OMe\text{-}Phimp)_2(Cl)_2]$ (**3**)

This compound was prepared by following the same procedure as described above for **1**, except using OMe-PhimpH instead of PhimpH. Yield: 71%. Anal. Calcd for $C_{38}H_{32}N_6Cl_2O_4Zn_2$: C, 54.44; H, 3.85; N, 10.02. Found: C, 54.10; H, 3.63; N, 10.35. IR (KBr pellets, cm^{-1}): ν(C=N), 1628, 1564, 1483, 1414, 1356, 1022, 652. UV–vis (CH_3CN $\lambda_{max,}$ nm (ε, in M^{-1} cm^{-1})): 391 (16451), 333 (22548), 303 (22225), 246 (28290).

6.3. Phosphatase activity

The dinuclear metal complexes show efficient phosphatase activity. Para-nitrophenylphosphate (PNPP) was utilized as the model substrate to explore the phosphatase activity. All experiments were carried out in 97.5% DMF/H_2O medium [43,44]. Solutions of the substrate 4-NPP and the zinc complexes were freshly prepared, and the total volume maintained was 3 mL. An initial screening of the hydrolytic tendency of all the metal complexes was performed until 2% formation of 4-nitrophenolate was reached and then the kinetic data were collected. The rate of hydrolysis of PNPP in the presence of zinc complexes **1**–**3** was measured spectrophotometrically by monitoring the UV absorption of the p-nitrophenolate anion at 423 nm as a function of time at 25 °C [44]. The investigation contained five sets, having a complex concentration of 0.05 mmol and substrate concentrations of 0.5 (10 equiv.), 0.7 (14 equiv.), 1.0 (20 equiv), 1.2 (24 equiv.) and 1.5 (30 equiv.) mmol. The stock solutions of 2 mM of the complexes and the substrate were set up in a DMF/H_2O mixture. The reactions were performed by injecting 50 μL of the complex and various volumes of the substrate (0.5, 0.74, 1.1, 1.34 and 1.7 mL) in a cuvette and making the final volume up to 3 mL with solvent. After complete mixing, the spectra were recorded at 25 °C, over 2 h at regular time intervals of 3 min, for all complexes. All the experiments were carried out at least twice, and average values were taken. The reactions were corrected for the extent of ionization of 4-nitrophenolate at 25 °C, utilizing the molar extinction coefficient for 4-nitrophenolate at 424 nm [43]. After three days the final A_∞ values for each set were obtained.

6.4. General procedure for benzoxazole synthesis

The Schiff base substrate (1 mmol) was dissolved in 5 mL acetonitrile. To this solution, 0.1 mol % of catalyst was added, then 3 mol% of TEMPO was added at room temperature. The reaction mixture was stirred at 60 °C for 12 h. The solvent was then evaporated, followed by addition of ethyl acetate. The reaction mixture was filtered and the filtrate was purified by column chromatography using silica gel (mesh size 60–120) and hexane as the eluent. The product yield was calculated based on the yield obtained after column chromatography. The NMR spectra of the compounds **3a**–**3e**, formed after catalysis, are shown in Figs. S12–S21.

6.5. NMR of the benzoxazole derivatives

2-Phenylbenzoxazole (3a): White solid. ^1H NMR (500 MHz, $CDCl_3$) δ, ppm: 8.27 (m, 2H), 7.79–7.77 (m, 1H), 7.60–7.58 (m, 1H), 7.54–7.53 (m, 3H), 7.36 (m, 2H). ^{13}C NMR (126 MHz, $CDCl_3$) δ, ppm: 163.0, 150.7, 142.1, 131.5, 128.9, 127.6, 127.2, 125.1, 124.5, 120.0, 110.6.

6-Methyl-2-phenylbenzoxazole (3b): White solid. ^1H NMR (400 MHz, $CDCl_3$) δ, ppm: 8.39 (q, J = 8.9 Hz, 4H), 7.60 (s, 1H), 7.50 (d, J = 8.3 Hz, 1H), 7.24 (d, J = 8.5 Hz, 1H), 2.51 (s, 3H). ^{13}C NMR (126 MHz, $CDCl_3$) δ, ppm: 157.1, 152.2, 142.3, 135.7, 133.3, 129.6, 128.8, 128.6, 120.0, 115.8, 114.9, 21.6.

6-Methoxy-2-phenylbenzoxazole (3c): White solid. ^1H NMR (500 MHz, $CDCl_3$) δ, ppm: 7.97 (m, 3H), 7.57 (t, J = 7.4 Hz, 2H), 7.46 (t, J = 7.7 Hz, 3H), 4.34 (s, 3H). ^{13}C NMR (126 MHz, $CDCl_3$) δ, ppm: 153.35, 146.79, 139.66, 134.82, 132.65, 131.02, 130.80, 130.22, 122.45, 115.83, 109.30, 20.00.

6-Chloro-2-phenylbenzoxazole (3d): White solid. ^1H NMR (500 MHz, $CDCl_3$) δ, ppm: 7.95–7.98(m, 3H), 7.58(t, J = 7.6 Hz, 2H), 7.47 (t, J = 7.6 Hz, 1H). ^{13}C NMR (125 MHz, $CDCl_3$) δ, ppm: 162.02,150.72, 141.08, 137.73, 129.22, 128.81, 125.30, 124.61, 120.05, 110.57.

6-Nitro-2-phenylbenzoxazole (3e): White solid. ^1H NMR (500 MHz, $CDCl_3$) δ, ppm: 8.44 (d, J = 8.7 Hz, 2H), 8.39 (d, J = 8.7 Hz, 2H), 7.83 (d, J = 7.2 Hz, 1H), 7.64 (d, J = 7.8 Hz, 1H), 7.46–7.40 (m, 2H). ^{13}C NMR (126 MHz, $CDCl_3$) δ, ppm: 160.6, 151.0, 141.9, 132.8, 128.4, 126.3, 125.2, 124.2, 120.7, 115.0, 110.9.

CRediT authorship contribution statement

Kapil Kumar: Conceptualization, Methodology. **Virendra Kumar Chaudhary:** . **U.P. Singh:** . **Kaushik Ghosh:** Supervision, Conceptualization, Writing - review & editing.

Declaration of Competing Interest

The authors declare that they have no known competing financial interests or personal relationships that could have appeared to influence the work reported in this paper.

Acknowledgements

K.G. is thankful to CSIR, New Delhi, India for financial assistance (01(2942)/18/EMR-II dated 01-05-2018). K.K. is thankful to UGC and V.K.C. is thankful to CSIR, India, for financial assistance. We are thankful for the Central Instrumental Facility, IIT Roorkee.

Appendix A. Supplementary data

Supplementary data to this article can be found online at https://doi.org/10.1016/j.poly.2021.115048.

References

[1] F.A. Cotton, G. Wilkinson, Advanced Inorganic Chemistry, 4th edn., Wiley Interscience, 1988, pp. 589–615.
[2] K. Ghosh, P. Kumar, N. Tyagi, U.P. Singh, Novel diphenoxo-bridged dinuclear zinc complexes: generation of phenoxyl-radical species and nuclease activity, Inorg. Chem. 49 (2010) 7614–7616.
[3] R. Sanyal, P. Chakraborty, E. Zangrando, D. Das, Phosphatase models: synthesis, structure and catalytic activity of zinc complexes derived from a phenolic Mannich-base ligand, Polyhedron 97 (2015) 55–65.
[4] H. Arora, S.K. Barman, F. Lloret, R. Mukherjee, Isostructural dinuclear phenoxo-/acetato-bridged manganese(II), cobalt(II) and zinc(II) complexes with labile sites: kinetics of transesterification of 2-hydroxypropyl-p-nitrophenylphosphate, Inorg. Chem. 51 (2012) 5539–5553.
[5] M. Sheoran, K. Bhar, T.A. Khan, A.K. Sharma, Synthesis and characterization of phenoxo-bridged dinuclear zinc(II) halide complexes: role of electron withdrawing group on phosphatase activity, J. Chem. Sci. 130 (2018) 1–10.
[6] R. Sanyal, X. Zhang, P. Kundu, T. Chattopadhyay, C. Zhao, F.A. Mautner, D. Das, Mechanistic implications in the phosphatase activity of mannich-based dinuclear zinc complexes with theoretical modeling, Inorg. Chem. 54 (2015) 2315–2324.
[7] B. Das, H. Daver, M. Pyrkosz-Bulska, E. Gumienna-Kontecka, F. Himo, E. Nordlander, An unsymmetric ligand with a N_5O_2 donor set and its corresponding dizinc complex: a structural and functional phosphoesterase model, Eur. J. Inorg. Chem. 2018 (2018) 4004–4013.
[8] M. Mitra, R. Singh, M. Pyrkosz-bulska, M. Haukka, E. Gumienna-kontecka, E. Nordlander, A bis (μ-phenoxo)-bridged dizinc complex with hydrolytic activity, Z. Anorg. Allg. Chem. 639 (2013) 1534–1542.
[9] R. Sanyal, S.K. Dash, S. Das, S. Chattopadhyay, S. Roy, D. Das, Catecholase activity, DNA cleavage and cytotoxicity of six Zn(II) complexes synthesized from designed Mannich ligands: higher reactivity of mononuclear over dinuclear, JBIC J. Biol. Inorg. Chem. 19 (2014) 1099–1111.
[10] A.K. Dhara, U.P. Singh, K. Ghosh, Radical pathways and O_2 participation in benzyl alcohol oxidation, and catechol and o-aminophenol oxidase activity studies with novel zinc complexes: an experimental and theoretical investigation, Inorg. Chem. Front. 3 (2016) 1543–1558.
[11] A.C. Deacy, C.B. Durr, J.A. Garden, A.J.P. White, C.K. Williams, Groups 1, 2 and Zn(II) heterodinuclear catalysts for epoxide/CO_2 ring-opening copolymerization, Inorg. Chem. 57 (2018) 15575–15583.
[12] C. Romain, J.A. Garden, G. Trott, A. Buchard, A.J.P. White, C.K. Williams, Di-zinc–aryl complexes: CO_2 insertions and applications in polymerisation catalysis, Chem. Eur. J. 23 (2017) 7367–7376.
[13] A. Thevenon, J.A. Garden, A.J.P. White, C.K. Williams, Dinuclear zinc salen catalysts for the ring opening copolymerization of epoxides and carbon dioxide or anhydrides, Inorg. Chem. 54 (2015) 11906–11915.
[14] S. Soobrattee, X. Zhai, K. Nyamayaro, C. Diaz, P. Kelley, T. Ebrahimi, P. Mehrkhodavandi, Dinucleating amino-phenolate platform for zinc catalysts: impact on lactide polymerization, Inorg. Chem. 59 (2020) 5546–5557.
[15] C. Fliedel, D. Vila-viåosa, J. Calhorda, S. Dagorne, Dinuclear zinc – N-heterocyclic carbene complexes for either the controlled ring-opening polymerization of lactide or the controlled degradation of polylactide under mild conditions, ChemCatChem 6 (2014) 1–12.
[16] J.A. Marafie, D.D.C. Bradley, C.K. Williams, Thermally stable zinc disalphen macrocycles showing solid-state and aggregation-induced enhanced emission, Inorg. Chem. 56 (2017) 5688–5695.
[17] A. Das, S. Jana, A. Ghosh, Modulation of nuclearity by Zn(II) and Cd(II) in their complexes with a polytopic Mannich base ligand: a turn-on luminescence sensor for Zn(II) and detection of nitroaromatic explosives by Zn(II) complexes, Cryst. Growth Des. 18 (2018) 2335–2348.
[18] (a) A. Hens, K.K. Rajak, Photophysical property vs. medium: Mononuclear, dinuclear and trinuclear Zn(II) complexes, RSC Adv. 5 (2015) 4219–4232;
(b) J.Z. Gu, Y. Cai, X.X. Liang, J. Wu, Z.F. Shi, A.M. Kirillov, Bringing 5-(3,4-dicarboxylphenyl)picolinic acid to crystal engineering research: Hydrothermal assembly, structural features, and photocatalytic activity of Mn, Ni, Cu, and Zn coordination polymers, CrystEngComm. 20 (2018) 906–916;
(c) J.Z. Gu, S.M. Wan, M.V. Kirillova, A.M. Kirillov, H-bonded and metal(ii)-organic architectures assembled from an unexplored aromatic tricarboxylic acid: structural variety and functional properties, Dalton Trans. 49 (2020) 7197–7209.
[19] S. Roy, S. Bhattacharya, S. Mohanta, Syntheses, crystal structures and photophysical aspects of discrete and polymeric azido-bridged zinc (II) and cadmium (II) complexes: sensing properties and structural resemblance, ChemistrySelect 2 (2017) 11091–11099.
[20] S. Yasuda, M. Takase, A. Sano, T. Akitsu, Schiff base dinuclear Zn(II) complexes as assisting fluorescent probe for CD19 antibody protein, Int. J. Chem. Eng. Appl. 8 (2017) 290–293.
[21] A. Tamilselvi, G. Mugesh, Zinc and antibiotic resistance: metallo-β-lactamases and their synthetic analogues, J. Biol. Inorg. Chem. 13 (2008) 1039–1053.
[22] L. Que, W.B. Tolman, Biologically inspired oxidation catalysis, Nature 455 (2008) 333–340.
[23] Y.X. Chen, L.F. Qian, W. Zhang, B. Han, Efficient aerobic oxidative synthesis of 2-substituted benzoxazoles, benzothiazoles, and benzimidazoles catalyzed by 4-Methoxy-TEMPO, Angew. Chem. Int. Ed. 47 (2008) 9330–9333.
[24] B.A. Jazdzewski, W.B. Tolman, Understanding the copper-phenoxyl radical array in galactose oxidase: contributions from synthetic modeling studies, Coord. Chem. Rev. 200–202 (2000) 633–685.
[25] K.A. Gardner, J.M. Mayer, Understanding C-H bond oxidations: H. and H-transfer in the oxidation of toluene by permanganate, Science 269 (1995) 1849–1851.
[26] P.U. Maheswari, S. Barends, S. Özalp-Yaman, P. De Hoog, H. Casellas, S.J. Teat, C. Massera, M. Lutz, A.L. Spek, G.P. Van Wezel, P. Gamez, J. Reedijk, Unique ligand-based oxidative DNA cleavage by zinc(II) complexes of hpyramol and hpyrimol, Chem. Eur. J. 13 (2007) 5213–5222.
[27] A. Guha, T. Chattopadhyay, N.D. Paul, M. Mukherjee, S. Goswami, T.K. Mondal, E. Zangrando, D. Das, Radical pathway in catecholase activity with zinc-based model complexes of compartmental ligands, Inorg. Chem. 51 (2012) 8750–8759.
[28] J. Perlstein, The Weak Hydrogen Bond In Structural Chemistry and Biology (International Union of Crystallography, Monographs on Crystallography, 9) By Gautam R. Desiraju (University of Hyderabad) and Thomas Steiner (Freie Universität Berlin). Oxford University Press: J. Am. Chem. Soc. 123 (2001) 191–192.
[29] G.R. Desiraju, The C-H···O hydrogen bond: structural implications and supramolecular design, Acc. Chem. Res. 29 (1996) 441–449.
[30] E.V. García-Báez, F.J. Martínez-Martínez, H. Höpfl, I.I. Padilla-Martínez, π-Stacking interactions and C-H···X (X = O, aryl) hydrogen bonding as directing features of the supramolecular self-association in 3-carboxy and 3-amido coumarin derivatives, Cryst. Growth Des. 3 (2003) 35–45.
[31] T. Lecklider, Maintaining a healthy rhythm, Phys. Rev. B EE Eval. Eng. 50 (2011) 36–39.
[32] N.M. O'Boyle, A.L. Tenderholt, K.M. Langner, Software News and updates cclib: a library for package-independent computational chemistry algorithms, J. Comput. Chem. 29 (2008) 839–845.
[33] (a) A. Erxleben, Mechanistic studies of homo- and heterodinuclear zinc phosphoesterase mimics: What has been learned?, Front Chem. 7 (2019) 1–22;
(b) K. Ghosh, P. Kumar, V. Mohan, U.P. Singh, S. Kasiri, S.S. Mandal, Nuclease activity via self-activation and anticancer activity of a mononuclear copper(II) complex: novel role of the tertiary butyl group in the ligand frame, Inorg. Chem. 51 (2012) 3343–3345.
[34] (a) K. Ghosh, S. Kumar, R. Kumar, U.P. Singh, N. Goel, Oxidative cyclization of a phenolic schiff base and synthesis of a cyclometalated ruthenium nitrosyl complex: photoinduced no release by visible light, Inorg. Chem. 49 (2010) 7235–7237;
(b) S. Enthaler, Rise of the zinc age in homogeneous catalysis?, ACS Catal 3 (2013) 150–158;
(c) S. Enthaler, X. Feng Wu, Zinc Catalysis: Applications in Organic Synthesis, John Wiley & Sons, 2015..
[35] N.U. Hofsløkken, L. Skattebøl, Convenient method for the ortho-formylation of phenols, Acta Chem. Scand. 53 (1999) 258–262.
[36] G.M. Sheldrick, Phase annealing in SHELX-90: direct methods for larger structures, Acta Crystallogr. Sect. A. 46 (1990) 467–473.
[37] P.J. Hay, W.R. Wadt, Ab initio effective core potentials for molecular calculations. Potentials for the transition metal atoms Sc to Hg, J. Chem. Phys. 82 (1985) 270–283.
[38] P.J. Hay, W.R. Wadt, Ab initio effective core potentials for molecular calculations. Potentials for K to Au including the outermost core orbitale, J. Chem. Phys. 82 (1985) 299–310.
[39] E.K.U. Gross, W. Kohn, Time-dependent density-functional theory, Adv. Quantum Chem. (1990) 255–291.
[40] (a) A.D. Becke, Density-functional thermochemistry. III. The role of exact exchange, J. Chem. Phys. 98 (1993) 5648–5652;
(b) T. Lecklider, Maintaining a healthy rhythm, EE Eval. Eng. 50 (2011) 36–39.
[41] T.K. and J.M. R. Dennington, Gauss View, Version 5, Semichem Inc., Shawnee Mission., 2009.
[42] M.J. Frisch, G.W. Trucks, H.B. Schlegel, G.E. Scuseria, M.A. Robb, J.R. Cheeseman, G. Scalmani, V. Barone, B. Mennucci, G.A. Petersson, H. Nakatsuji, M. Caricato, X. Li, H.P. Hratchian, A.F. Izmaylov, J. Bloino, G. Zheng, J.L. Sonnenberg, M. Hada, M. Ehara, K. Toyota, R. Fukuda, J. Hasegawa, M. Ishida, T. Nakajima, Y. Honda, O. Kitao, H. Nakai, T. Vreven, Jr. J.A. Montigomery, J.E. Peralta, F. Ogliaro, M. Bearpark, J. J. Heyd, E. Brothers, K.N. Kudin, V.N. Staroverov, T. Keith, R. Kobayashi, J. Normand, K. Raghavachari, A. Rendell, J. C. Burant, S.S. Iyengar, J. Tomasi, M. Cossi, N. Rega, J.M. Millam, M. Klene, J.E. Knox, J.B. Cross, V. Bakken, C. Adamo, J. Jaramillo, R. Gomperts, R.E. Startmann, O. Yazyev, A.J. Austin, R. Cammi, C. Pomelli, J. W. Ochterski, R.L. Martin, K. Morokuma, V.G. Zakrzewski, G.A. Voth, P. Salvador, J. J. Dannenberg, S. Dapprich, A.D. Daniels, O. Farkas, J.B. Foresman, J.V. Ortiz, J. Cioslowski, D.J. Fox, Gaussian 09, Revision A01, Gaussian, Inc.: Wallingford, CT, 2009.
[43] M. Subat, K. Woinaroschy, S. Anthofer, B. Malterer, B. König, 1,4,7,10-Tetraazacyclododecane metal complexes as potent promoters of carboxyester hydrolysis under physiological conditions, Inorg. Chem. 46 (2007) 4336–4356.
[44] R. Sanyal, A. Guha, T. Ghosh, T.K. Mondal, E. Zangrando, D. Das, Influence of the coordination environment of zinc(II) complexes of designed Mannich ligands on phosphatase activity: a combined experimental and theoretical study, Inorg. Chem. 53 (2014) 85–96.